JOURNAL OF PROPULSION AND POWER
Vol. 11, No. 2, March–April 1995

Mixing and Penetration Studies of Sonic Jets in a Mach 2 Freestream

M. R. Gruber* and A. S. Nejad†
U.S. Air Force Wright Laboratory, Wright–Patterson Air Force Base, Ohio 45433
T. H. Chen‡
Taitech Group, WL/POPT, Wright–Patterson Air Force Base, Ohio 45433
and
J. C. Dutton§
University of Illinois at Urbana–Champaign, Urbana, Illinois 61801

A comparison of the penetration and mixing characteristics of three transverse/oblique injector configurations is presented. The three geometries studied include circular transverse, circular oblique, and elliptical transverse injectors, and the crossflow is at Mach 2. Planar Mie scattering images of three near-field flow planes produced substantial information about the flowfield created by each injector. In addition to global flowfield characteristics, the Mie scattering images provided transverse and lateral penetrations for each injector. Instantaneous and time-averaged information concerning the structural organization of the flowfields was obtained. Results demonstrate increasing jet penetration in the transverse direction with increasing jet-to-freestream momentum flux ratio. Penetration of the oblique jet is appreciably less in the near-field compared to the two transverse jets due to the reduced component of momentum in the transverse direction. The transverse elliptic jet appears to spread more quickly in the lateral direction than the other two jets, suggesting that some type of axis-switching phenomenon occurs. Large-scale structures at the interface between the jet and freestream fluids are shown for the two transversely oriented jets, while small-scale eddies are prominent in the oblique jet flowfield. Near-field mixing appears dominated by these eddies and the counter-rotating structures that develop in the streamwise direction.

Nomenclature

A = area
a = semimajor axis of an ellipse
b = semiminor axis of an ellipse
d_{eff} = effective injector diam, $(4A_{\text{xs}}/\pi)^{1/2}$
d_p = particle diameter
J = jet-to-freestream momentum flux ratio
Kn = Knudsen number (ratio of mean free path to particle diameter)
M = Mach number
p = static pressure
T_0 = total temperature
t_p = particle response time
t_δ = large eddy rollover time
u = velocity
x = streamwise coordinate
y = transverse coordinate
z = spanwise coordinate
γ = specific heat ratio
δ = boundary layer thickness, shear layer vorticity thickness
ε = eccentricity
μ = dynamic viscosity
ρ = density

Subscripts
ex = exit
f = freestream
j = jet
p = particle
xs = cross section

Received Dec. 20, 1993; presented as Paper 94-0709 at the AIAA 32nd Aerospace Sciences Meeting, Reno, NV, Jan. 10–13, 1994; revision received July 13, 1994; accepted for publication Aug. 9, 1994.

*Aerospace Engineer, Advanced Propulsion Division, Experimental Research Branch. Member AIAA.
†Senior Research Engineer, Advanced Propulsion Division, Experimental Research Branch.
‡Senior Research Scientist. Senior Member AIAA.
§Professor, Department of Mechanical and Industrial Engineering. Associate Fellow AIAA.

Introduction

FUNDAMENTAL to the success of hypersonic air-breathing propulsion systems are the efficient injection, mixing, and combustion processes that occur inside the combustion chamber. These processes will take place in a supersonic stream, and thus, must occur quickly because residence times within such combustors will necessarily be short, even when fuel dispersion is aided by such intrusive features as struts or ramps. The transverse jet injected into a supersonic crossflow represents a possible configuration for fuel delivery in such engines.

Many early investigations of the transverse gaseous jet in supersonic crossflow revolved around qualitative examinations of the underexpanded injection flowfield and analytical descriptions of the injectant penetration depth as a function of various flow parameters.[1,2] Schlieren photographs of the injection flowfield revealed the presence of a bow shock wave upstream of the injector exit, rapid turning of the injectant gas, a Mach disk, and regions of recirculating flow immediately upstream and downstream of the jet orifice. Figure 1 is a schematic representation of the flowfield.

One analytical model developed for the prediction of jet penetration assumed that the sonic jet issues into a stream with no boundary layer and that no mixing occurs between the injectant and freestream fluids near the injector orifice.[1] A momentum balance applied to a prescribed plume geometry resulted in a functional form for the penetration depth that accurately predicted the jet penetration determined from the

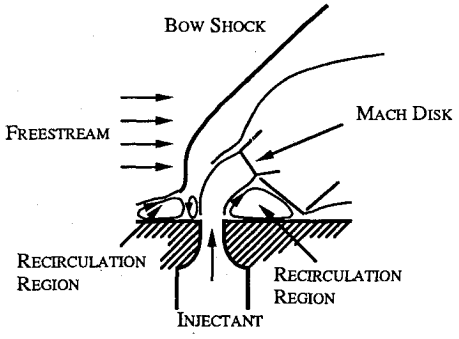

Fig. 1 Transverse injection flowfield schematic.

measured maximum injectant concentration profile. A similar model developed in another study[2] resulted in an expression for the penetration that suggested that the jet-to-freestream momentum flux ratio (or dynamic pressure ratio), given by

$$J = \frac{(\rho u^2)_j}{(\rho u^2)_f} = \frac{(\gamma p M^2)_j}{(\gamma p M^2)_f} \tag{1}$$

was the principal controlling parameter. Another concept introduced in this study was that of the "effective back pressure" seen by the jet. This pressure, analogous to the back pressure in the flowfield formed by a jet issuing into a quiescent environment, is the average pressure in the near-jet region. The complex nature of the pressure field surrounding the injector orifice in this flow makes it difficult to determine an accurate effective back pressure when using conventional methods. Schetz and Billig[2] suggested that injection at a pressure-matched condition (i.e., where the static pressure of the jet is equal to the effective back pressure) produced a more optimum penetration than simply overpressurizing the jet, due to reduced shock losses.

Recent studies investigated the issue of penetration more fully.[3,4] Papamoschou and Hubbard[3] examined the effects of freestream and jet Mach numbers, static pressure and density ratios, and momentum flux ratio on penetration using schlieren photography. Results indicated that the jet's penetration into the supersonic crossflow was principally dependent on the momentum flux ratio defined in Eq. (1). They found little or no effect due to the freestream or jet Mach numbers, while evidence of an optimum penetration at a certain pressure ratio provided support for the matched pressure condition cited above.[2] Rothstein[4] used planar laser-induced fluorescence (PLIF) to study transverse injection of hydrogen into a Mach 1.5 oxygen crossflow. A power law fit to the penetration data was proposed. The constants in the power law expression have been determined by numerous authors and are found to vary widely between studies.

In addition to the extent of jet penetration, the issue of jet/freestream mixing is of critical importance for hypersonic propulsion applications. This issue has been addressed by using a concentration probe and PLIF of iodine.[1,5] The results of the former study suggested that streamwise vortices generated at either side of the jet play an important role in the near-field mixing process. Time-averaged mole fraction images obtained from a complex staged injector flowfield[5] demonstrated rapid mixing in the region between the two injectors, while the mixing just downstream of the second injector appeared strongly influenced by streamwise vorticity. These vortices, which arise from vorticity in the boundary layer of the injectant fluid,[6] appear very prominently in incompressible transverse injection flowfields,[7] where both the temperature and velocity fields are significantly affected by their presence.

Structural organization within a flow can have direct implications on its mixing characteristics, as in the fully developed compressible shear layer.[8,9] Recent transverse jet studies made note of the large-scale structures that formed at the interface between the freestream and injectant fluids.[10,11] These structures persisted until far downstream and appeared to occur on a somewhat regular basis. Two-dimensional acetone PLIF images taken of a subsonic jet injected into a subsonic crossflow revealed similar large-scale behavior.[12]

One drawback to transverse injection is the stagnation pressure loss due to the relatively strong bow shock present just ahead of the injector. This issue was addressed in two studies where the effects of injection at low transverse angles to the freestream were examined.[13,14] Reduced total pressure losses resulted due to the weaker bow shock produced. Results from Fuller et al.[14] indicate that for low angle injection ($\theta = 30$ and $\theta = 15$ deg), an increase in injection angle (combined with fixed jet pressure-to-effective back pressure ratio) produces a faster mixing rate in the near field due to the increased disturbance felt by the freestream. However, in the far field, the peak injection concentrations of the two cases are nearly equal. Transverse and oblique mixing data have been compiled by Schetz et al.[15] and the results presented demonstrate similar conclusions, i.e., that increases in injection angle of oblique jets produce faster mixing in the near-field, larger total pressure losses due to increased disturbance effects, and no mixing advantage in the far field over the lower angle counterparts.

Studies of a small aspect ratio elliptical jet showed that the boundary-layer momentum thickness varied around the nozzle circumference leading to the development of asymmetric vortices at the exit plane.[16,17] In quiescent and coflowing environments, spreading rates in the minor-axis plane of the elliptical jet were faster than those associated with the major-axis plane. This eventually led to the minor-axis spread being larger than the major-axis spread (a phenomenon termed axis-switching). Further spreading enhancement occurs in underexpanded elliptical jets compared to those operated perfectly expanded (sonic) or subsonic.[18]

This investigation is a comparison of the near-field mixing and penetration characteristics of three basic injector geometries. Planar Mie scattering is used to study the flowfields created by jets issuing from circular transverse, circular oblique, and elliptical transverse injectors into a Mach 2 crossflow. Of specific interest are the transverse and lateral spread of the jet from each injector, and the instantaneous and time-averaged structural behavior of the jet/freestream interface. Examination of the jet's penetration, both transversely and laterally into the freestream, allows conclusions to be drawn concerning the effectiveness of the injection process and the effects of both injector geometry and orientation. Investigation of the jet/freestream interfacial structure will lead to qualitative interpretations of the mixing characteristics of each injector by revealing the large- and small-scale motions characteristic of each. Finally, this work will be used as a baseline for future, more exhaustive studies of the three injection flowfields.

Experimental Facility

The experiments documented herein were performed in a newly constructed supersonic combustion research facility located at Wright-Patterson Air Force Base. The various components of this facility, as well as quantitative flow quality measurements, have been discussed in great detail elsewhere[19]; only a summary of the important features is included here.

Flow Facility

The wind tunnel used in this investigation is shown schematically in Fig. 2. A series of compressors capable of producing a continuous 34-lbm/s flow of air at about 750 psig and ambient temperature supplied the facility. Additionally, an exhauster system evacuated the test section to approximately 3 psia before starting the tests.

A rearward-facing perforated cone, along with an array of mesh screens and a section of honeycomb, conditioned the

Table 1 Injector geometries

Injector	a, in.	b, in.	A_{xs}, in.^{2}	A_{ex}, in.^{2}	ε
1	0.125	0.125	0.049	0.049	0
2	0.483	0.125	0.049	0.190	0.97
3	0.246	0.064	0.049	0.049	0.97

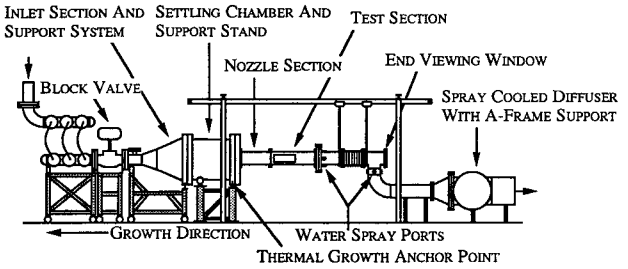

Fig. 2 Schematic of supersonic combustion tunnel.

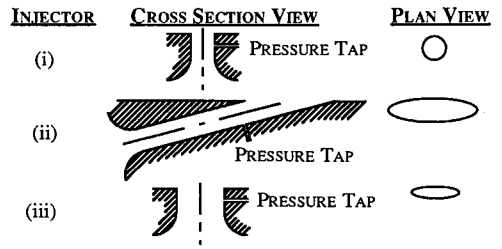

Fig. 3 Illustration of injector configurations used in the present study.

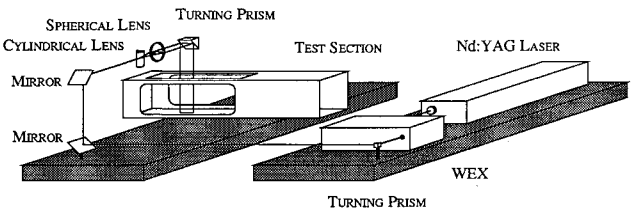

Fig. 4 Mie scattering optical arrangement.

air within the settling chamber. The cone spread the flow uniformly within the chamber while the screens and honeycomb served to reduce large-scale turbulence and straighten the flow before acceleration by the supersonic nozzle. Tunnel stagnation conditions were monitored by a Johnson-Yokogawa control system used for feedback and control of the various valves in the system.

The present investigation used a nozzle section designed with a method of characteristics code[20] to produce a nominally Mach 2 freestream. Results of a recent effort to characterize the tunnel indicated that the flow is uniform and two dimensional within the test section at a Mach number of about 1.98.[19] The cross-sectional dimensions of the constant area test section used in these studies were 5 in. by 6 in. A number of fused quartz windows, including a pair of side windows, a top window, and an end window, provided optical access to the flow. The resulting access to the flow allowed direct imaging of three orthogonal flow planes.

For the present study, injector geometries were incorporated into the removable test inserts housed within the bottom wall of the test section. Five streamwise positions were available for injector placement. For this study, all injectors were placed at the same streamwise location to ensure that the boundary-layer thickness approaching the injector would be the same for each case. At the chosen injector location, the boundary-layer thickness-to-effective jet diameter ratio is approximately $\delta/d_{\text{eff}} = 1$.

Injectors

The three injector geometries designed for these experiments included 1) a circular jet issuing transversely, $\theta = 90$ deg, 2) a circular jet issuing obliquely, $\theta = 15$ deg, and 3) an elliptical jet issuing transversely, $\theta = 90$ deg. To ensure a proper comparison among the three injectors, each had a cross-sectional area (i.e., area perpendicular to the jet axis) of 0.049 in.^{2}. The orifice diameter of injector 1 was, therefore, 0.25 in. An additional constraint on injectors 2 and 3 was that the elliptical geometries at the nozzle exits be similar. Equating the eccentricities of the ellipses and the cross-sectional areas of the supply tubes allowed this constraint to be met. Table 1 presents the geometries of the injectors, where the eccentricity ε is

$$\varepsilon = \sqrt{1 - (b^2/a^2)} \tag{2}$$

and a and b are the semimajor and semiminor axes, respectively. Figure 3 illustrates the cross-sectional and plan views of the injector geometries. The resulting injectors have the same effective diameter ($d_{\text{eff}} = 0.25$ in.), whereas the exit area of the circular oblique injector differs from that of the other two.

Each injector was equipped with a pressure tap near the exit, as shown in Fig. 3, for static pressure measurements. A bank of Pressure Systems Incorporated pressure transducers controlled by a 386-PC acquired pressure data from the injectors. In addition to this, the jet stagnation temperature was measured just upstream of the entrance to each injector using a thermocouple that was monitored visually. Both readings allowed the operating conditions of the injectant flow to be set.

Dry carbon dioxide and helium served as injectant gases in these studies. The CO_2 was supplied to the injector using a manifold system of five bottles. A high mass flow hand regulator was used to set injectant pressures, and a 50-gal hot water bath and resistive heat tape heated the copper supply line. The energy supplied by the heaters maintained the jet stagnation temperature at roughly 540°R. Helium was supplied through a separate line using a 66,000-ft^3 trailer pressurized to 2000 psig. Helium pressures and temperatures were regulated with the same systems as for the carbon dioxide.

Imaging System

A Spectra Physics Quanta-Ray DCR-4 Nd:YAG laser with an 8-ns pulse duration provided the laser beam used in these experiments. The laser pulsed at 10 Hz and a second harmonic generator frequency doubled the 1064-nm beam to 532 nm. This beam was again frequency doubled by a WEX system to produce UV light at 266 nm (approximately 90 mJ/pulse). A prism directed the beam from the laser table to the traversing table positioned beneath the test section. A pair of coated mirrors reflected the beam up and toward the test section at the desired elevation. Finally, a cylindrical/spherical lens system produced the thin laser sheet used for illuminating the desired flow plane. Figure 4 provides a schematic illustration of the laser system used in these experiments.

The unintensified CCD camera and image acquisition system used here were manufactured by Princeton Instruments. The camera was water cooled and purged with dry nitrogen to reduce dark count noise. A Nikon UV-Nikkor 105-mm f/4.5 telephoto lens was used for imaging the 266-nm Mie scattering from naturally occurring ice crystals in the freestream, which provided a "scalar transport" seeding arrangement.[8,21] Studies of condensation inside supersonic nozzles have shown that the ice crystals formed were nearly monodisperse with diameters between 0.003–0.014 μm, depending on the humidity of the inlet air.[22,23] Accurate particle response

Table 2 Image acquisition details

View	J	Injector	Injectant	Image plane location
Side	1, 2, 3	1, 2, 3	He, CO_2	$z/d_{eff} = 0$
Top	3	1, 2, 3	He, CO_2	$y/d_{eff} = 2$
End	3	1, 2, 3	He, CO_2	$x/d_{eff} = 2, 5$

for Mie scattering images requires a Stokes number, defined by

$$\text{Stokes number} = \frac{t_p}{t_\delta} = \frac{\text{particle response time}}{\text{large eddy rollover time}} \quad (3)$$

of less than about 0.5 (Ref. 24). The two time scales involved in determining the Stokes number are

$$t_p = (1 + 2.76 \cdot Kn)\frac{\rho_p d_p^2}{18\mu} \quad \text{and} \quad t_\delta = \frac{\delta}{\Delta U} \quad (4)$$

Using a conservative ice crystal diameter of 0.02 μm and an average velocity difference between the jet and freestream fluids of 400 m/s yields a Stokes number of 0.003 for the present operating conditions, thereby indicating that the crystals easily follow the turbulent fluctuations within this flowfield. The resulting images were characterized by high intensity values in pure freestream regions and low intensities in regions of pure injectant. A Princeton Instruments pulse generator provided synchronization between the flash lamp of the laser and the camera, and the camera was gated to visualize one entire laser pulse. The 384 × 576 pixel density of the CCD array, combined with the optical arrangement described, produced spatial resolutions of 125 μm/pixel in the side view images, 65 μm/pixel in the top view images, and 460 μm/pixel in the end view images. Each 14-bit image was sent to a 486-PC for preliminary analysis, display, and storage. Side view images were collected at $J = 1$, 2, and 3 for each injector and both injectant gases. Top and end view images were collected for each injector and both gases at $J = 3$. Table 2 contains details concerning the various image plane locations used here.

Further analysis of the images was performed on the 486-PC and a Macintosh Quadra. Normalized averages were computed and corrected for reflections and nonuniformities in both the CCD array and laser sheet for each of the three image planes. To carry out the correction procedure, 10 background images (taken with no flow) for each case were averaged and the average was subtracted from each of 10 laser sheet profiles (taken with freestream flow only) and 10 instantaneous jet images. These corrected beam profiles and jet images were then averaged. The average beam profile was divided out of the average jet image and the resulting corrected jet image was then normalized by the maximum intensity within the image. This procedure was carried out for each flow condition. Other image processing was completed and is discussed below.

Results and Discussion

Experimental conditions for the present study are listed in Table 3. Notice that the static pressure within the test section was held constant while jet operating conditions were adjusted to provide the desired jet-to-freestream momentum flux ratio. Global flowfield characteristics were visualized using the Mie scattering technique. Intensity contours defined in the various averaged images were used to provide quantitative information about the transverse and lateral penetration of the three injector geometries. In addition, analysis of the instantaneous images gave information about the structural behavior of the jet/freestream interface region and qualitative characteristics

Table 3 Experimental flow conditions ($T_{0,f}$ = 560–580°R)

J	Injectant	M_f	M_j	p_f, psia	p_j, psia	γ_j
1	CO_2	2.0	1.0	5.3	23.0	1.29
1	He	2.0	1.0	5.3	17.8	1.67
2	CO_2	2.0	1.0	5.3	46.0	1.29
2	He	2.0	1.0	5.3	35.5	1.67
3	CO_2	2.0	1.0	5.3	69.0	1.29
3	He	2.0	1.0	5.3	53.3	1.67

Fig. 5 Instantaneous side view image; elliptical, 90-deg injector, CO_2.

of the near-field mixing. These results are addressed individually below.

Global Flowfield Characteristics

Planar imaging techniques, such as the Mie scattering used here, result in two-dimensional images containing intensity information. Figure 5 shows a typical instantaneous side view image of a CO_2 jet formed using the elliptical transverse injector. The location of the injector appears at the bottom of the image. Freestream fluid, characterized by high signal (white), contained the ice crystals used for scattering. The jet fluid appears black/gray except within the barrel shock region. This apparent anomaly will be discussed below. The three-dimensional bow shock upstream of the injector is clearly visible in the figure. From shot-to-shot, the bow shock appeared to be stationary with no large fluctuations in position.

The interface between the jet and the freestream is especially interesting. The presence of large-scale structures is immediately apparent. The orientation of these structures, i.e., rolling up into the freestream fluid, implies that the jet fluid at the boundary moves with a higher velocity tangent to the interface than the freestream fluid. This tendency is clearly evident in studies of planar shear layers.[8,9] A final feature of the image in the figure is the appearance of the barrel shock and Mach disk within the underexpanded jet. These features are not visible in the cases where helium is used, and are most prominent in CO_2 images at high J. Based on models of the barrel shock/Mach disk region[2,25] and the thermodynamic characteristics of carbon dioxide,[26] it is thought that as the injectant accelerates into the freestream the CO_2 undergoes a phase change from gas to solid due to the drop in temperature and pressure. The frozen CO_2 is then able to scatter laser light and thus appears as white in the image. Signal is lost downstream of the Mach disk as the frozen carbon dioxide is sublimated due to the sudden compression (and increase in both temperature and pressure).

Transverse and Lateral Penetration

Defining the extent of jet penetration requires an objective reference to judge different cases fairly. Since the freestream fluid contained the scattering medium, an average freestream intensity value from the region downstream of the bow shock provided this reference. The averaged side and end view images allowed a clear definition of the freestream region downstream of the bow shock making intensity averages from within this zone possible. However, the top view images were ob-

tained at locations too near the bottom wall so that no freestream fluid behind the bow shock was available for referencing. Also, due to the confusion associated with the condensation of carbon dioxide, transverse and lateral penetration data only result from the side and end view images using helium as the injectant.

Transverse Penetration

Figures 6a–6c illustrate the results of analyzing the averaged side view images for jet penetration. The intensity of the jet boundary presented corresponds to 90% of the average freestream intensity behind the bow shock (i.e., outer edge of the jet). Each of the plots compares the performance of an individual injector configuration with increasing jet-to-freestream momentum flux ratio, using helium as the injectant. The injector locations are illustrated in the figures by the shaded boxes beneath the horizontal axes. Figure 6a compares the penetration profiles of the circular 90-deg injector for values of J ranging from 1 to 3. The plot provides evidence for the expected trend of increasing transverse penetration with increasing J. Peak transverse penetration in the high J case for the field of view provided by the laser sheet is about $y/d_{\text{eff}} = 4.2$ at $x/d_{\text{eff}} = 5.0$. Further increases in transverse penetration are expected downstream of this location since the asymptotic value of y/d_{eff} for circular transverse injectors occurs near $x/d_{\text{eff}} = 8$.[3]

The penetration profiles of the circular 15-deg injector are shown in Fig. 6b for values of J ranging from 1 to 3. The same trend of increasing jet penetration with increasing J is evident, although the extent of penetration is suppressed due to the smaller component of transverse momentum associated with the oblique injection geometry. A peak value of about $y/d_{\text{eff}} = 2.4$ at $x/d_{\text{eff}} = 5.0$ is found for $J = 3$. The slopes of the profiles at the downstream edge of the plot suggest, however, that the jet has not reached its full extent of penetration. Notice that the exit geometry of this injector is such that the laser sheet only allows examination of one effective diameter downstream of the trailing edge of the exit.

Figure 6c presents the transverse penetration profiles obtained for the elliptical 90-deg injector. Again, the trend of deeper penetration into the freestream with increased J is clearly observed. A peak penetration value of $y/d_{\text{eff}} = 4.0$ at $x/d_{\text{eff}} = 4.5$ is observed for $J = 3$. This value is close to the peak penetration obtained from the circular 90-deg injector. The jet cross-sectional shape does not appear to impact the extent of transverse penetration of the two transversely oriented jets substantially under the current conditions.

Keffer and Baines[27] found that the penetration profile data obtained from a subsonic jet in crossflow collapsed to a single curve in the near injector region when the coordinate axes were scaled by J^{-1}. Figure 6d illustrates the results of such a scaling on the profiles obtained in the current investigation. Clearly, the profiles demonstrate a high degree of collapse. The resulting power law fit is of the form

$$(y/d_{\text{eff}} \cdot J) = 1.23(x/d_{\text{eff}} \cdot J)^{0.344} \tag{5}$$

The correlation coefficient obtained from this fit was over 98%. Figure 6e compares the results of this correlation (for a momentum flux ratio of 3) to others obtained from PLIF studies.[4,28] The plot demonstrates very good agreement at this value of J. Although not shown, similar agreement was found for the $J = 2$ case while the present correlation fell below both referenced curves for $J = 1$. Figures 6d and 6e suggest that the present method for determining the jets' penetration profiles produces adequate results for comparison with other results found in the literature.

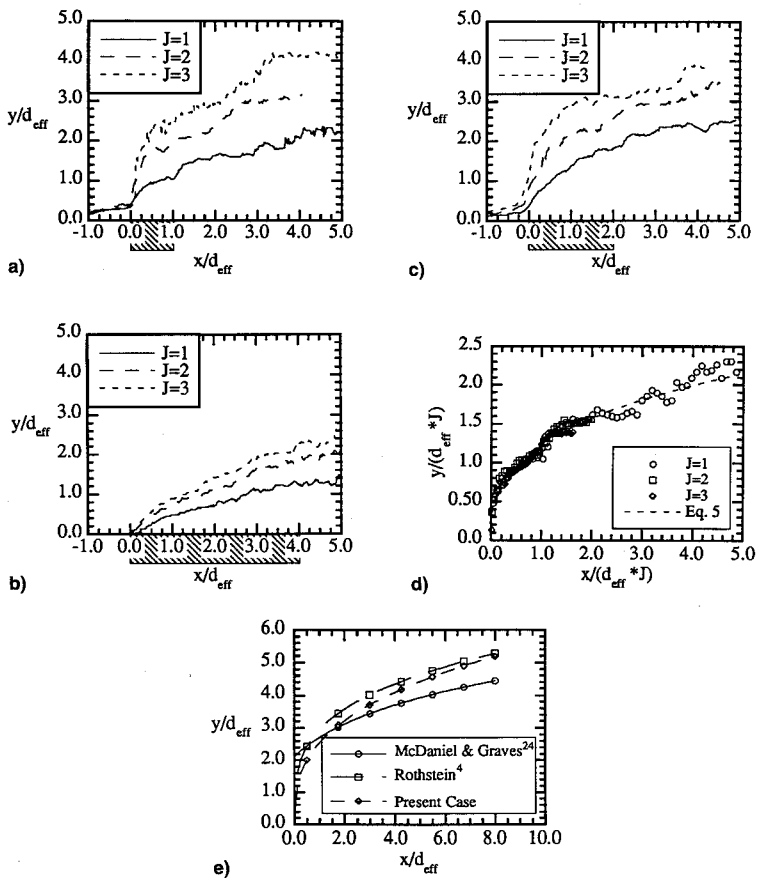

Fig. 6 Transverse jet penetration profiles: a) circular, 90-deg injector, He; b) circular, 15-deg injector, He; and c) elliptical, 90-deg injector, He. Collapse of transverse penetration profiles: d) circular, 90-deg injector, He and e) comparison of empirical correlations; circular, 90-deg injector, $J = 3$.

Lateral Penetration

Contours taken from averaged end view images using helium as the injectant are presented in Figs. 7–9. As with the previously discussed side view penetration profiles, these contours correspond to intensity values equal to 90% of the averaged freestream intensity downstream of the bow shock. Shown in Fig. 7 are the two contours obtained using the circular 90-deg injector with the image planes located at $x/d_{eff} = 2$ (Fig. 7a) and 5 (Fig. 7b). Figure 7a shows the lateral extent (i.e., extent in the z direction) covering roughly $z/d_{eff} = 3.6$. At the downstream location (Fig. 7b), the jet separates from the wall, and the lobes near the wall suggest the characteristic counter-rotating streamwise vortical structure present in the injectant. Further discussion of this feature is given in the following section. The lateral extent shown here is about $z/d_{eff} = 3.4$. Thus, the jet appears to contract laterally somewhat in the near-field region of this flowfield. The contours do exhibit transverse growth as expected.

Figures 8a and 8b illustrate the lateral and transverse spread of the obliquely oriented injector for the same streamwise image planes as Fig. 7. Again, due to the oblique geometry, transverse penetration is small for this injector compared to the previous contours for the 90-deg circular injector. Additionally, the lateral spread attributed to this injector is smaller in the near field compared to injector 1. Here, a lateral spread of about $z/d_{eff} = 2.9$ is revealed. Figure 8b again illustrates the lobes that develop as the jet lifts from the wall, suggesting that streamwise-oriented counter-rotating structures are found in this flowfield also.

End view contours obtained for the elliptical 90-deg injector are shown in Figs. 9a and 9b. Immediately visible in the first plot is the fuller nature of the penetration contour than any of those previously discussed. Lateral penetration is roughly $z/d_{eff} = 4.5$. A slightly smaller extent (roughly $z/d_{eff} = 4.2$) results from Fig. 9b, indicating again that the jet appears to contract laterally somewhat in the near field. The contour in Fig. 9b also suggests the same counter-rotating nature of the eddies on either side of the injector orifice as seen for the other injectors. An interesting note on the contours presented in Fig. 9 is that the elliptical orifice of injector 3 has about half the span of the circular orifice of injector 1 (see "*b*" of Table 1), while its lateral penetration is 25% larger. This indicates that the flow leaving the elliptical 90-deg injector spreads very quickly (in the lateral direction) in the near field compared to the circular 90-deg injector, suggesting that the axis-switching phenomenon discussed above[17] may be preserved in this flowfield.

Structural Behavior/Mixing

Select instantaneous images of the three views are shown in Figs. 10–12. All images presented are at $J = 3$ with carbon dioxide or helium used as the injectant as indicated. Injector

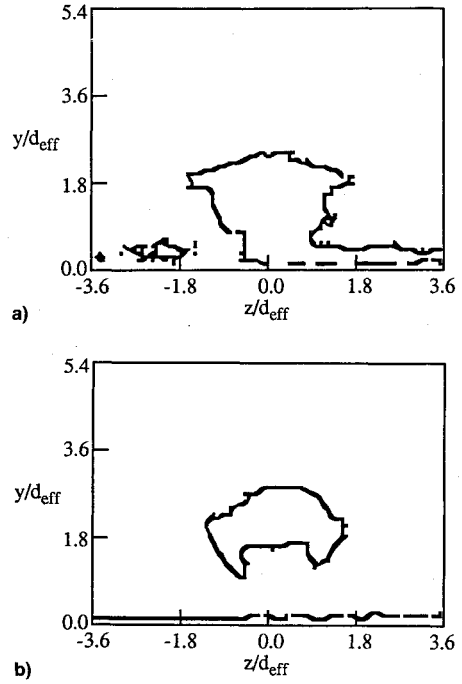

Fig. 8 Lateral penetration profiles: a) circular 15-deg injector at $x/d_{eff} = 2$, He at $J = 3$ and b) circular 15-deg injector at $x/d_{eff} = 5$, He at $J = 3$.

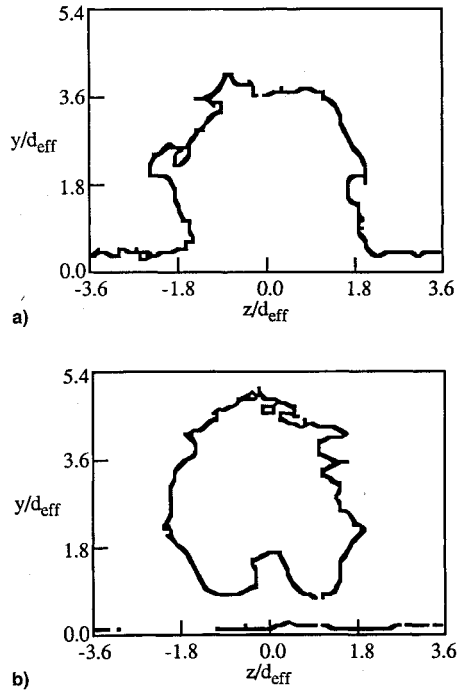

Fig. 7 Lateral penetration profiles: a) circular 90-deg injector at $x/d_{eff} = 2$, He at $J = 3$ and b) circular 90-deg injector at $x/d_{eff} = 5$, He at $J = 3$.

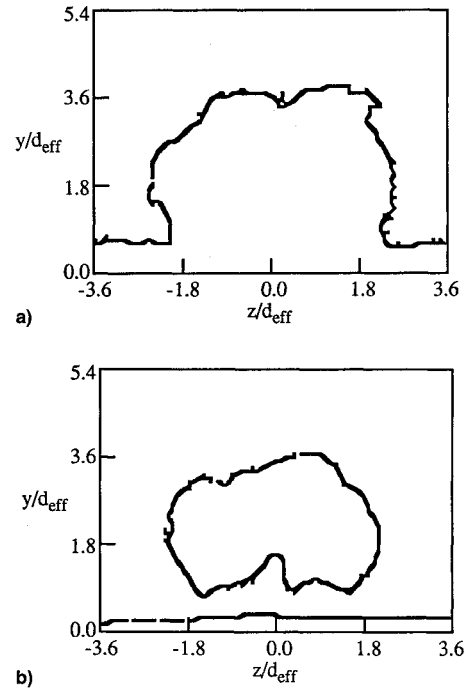

Fig. 9 Lateral penetration profiles: a) elliptical 90-deg injector at $x/d_{eff} = 2$, He at $J = 3$ and b) elliptical 90-deg injector at $x/d_{eff} = 5$, He at $J = 3$.

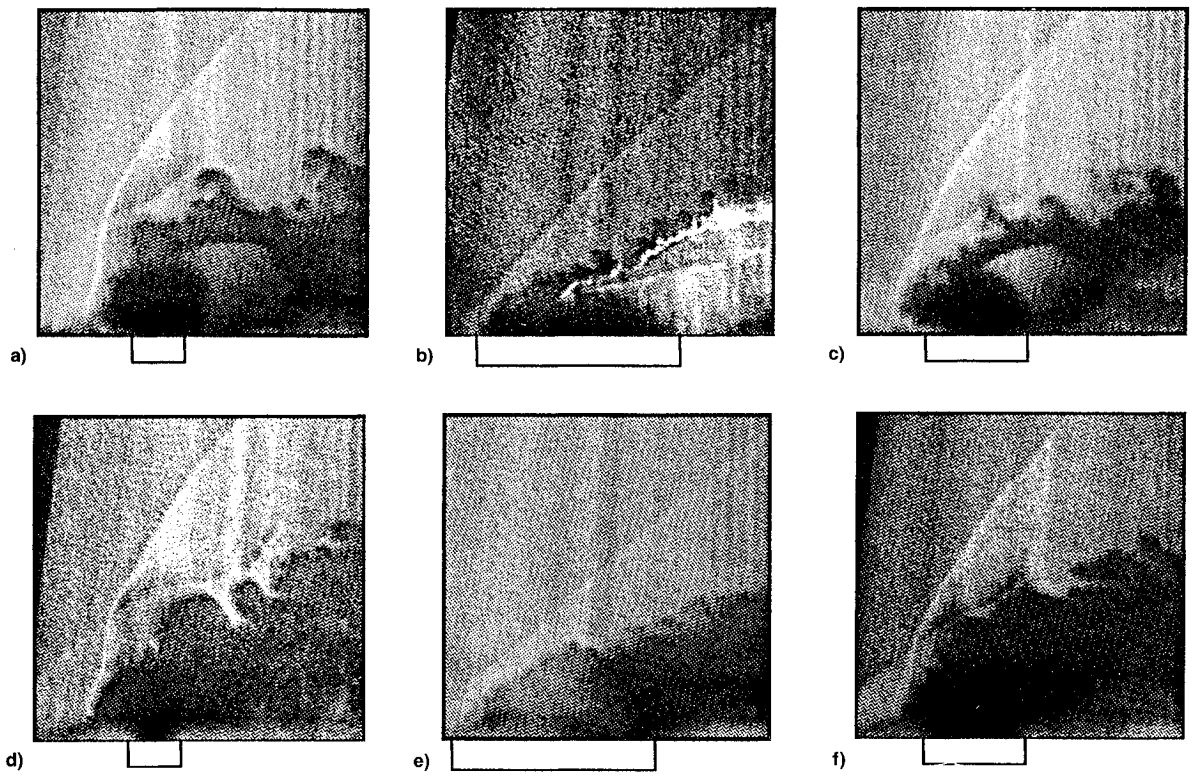

Fig. 10 Side view Mie scattering images at $J = 3$: a) circular 90-deg injector, CO_2; b) circular 15-deg injector, CO_2; c) elliptical 90-deg injector, CO_2; d) circular 90-deg injector, He; e) circular 15-deg injector, He; and f) elliptical 90-deg injector, He.

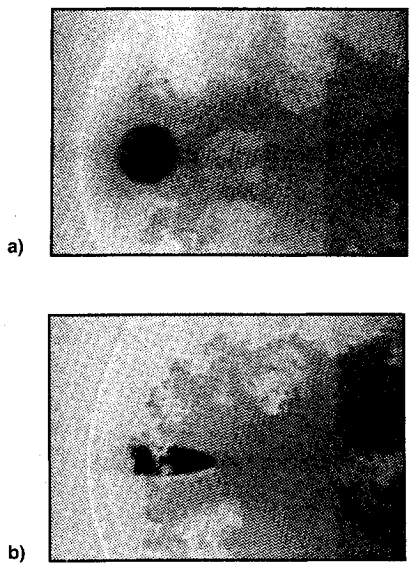

Fig. 11 Top view Mie scattering images at $J = 3$: a) circular 90-deg injector, CO_2 and b) elliptical 90-deg injector, CO_2.

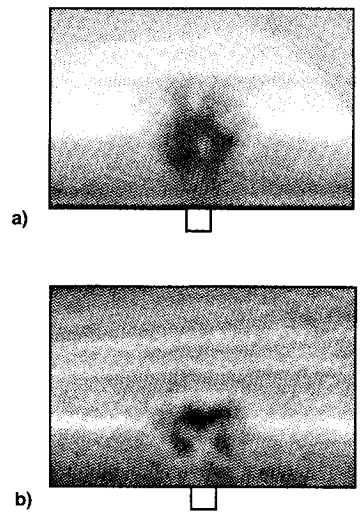

Fig. 12 End view Mie scattering images at $J = 3$: a) circular 90-deg injector; He at $x/d_{\text{eff}} = 2$ and b) circular 15-deg injector; He at $x/d_{\text{eff}} = 5$.

locations appear as rectangles at the bottom of each side and end view image. Flow is from left to right in Figs. 10 and 11, whereas the flow direction is out of the page in Fig. 12. As described for Fig. 5, the seeded freestream appears white while the unseeded jet appears black/gray, except where frozen carbon dioxide is present.

Side view images of the near field of the three injectant flowfields are presented in Fig. 10, where one image from the elliptical 90-deg injector is repeated from Fig. 5 for comparison. Each of the six images displays a region approximately 1.5 in. in the streamwise direction by 1.5 in. in the transverse direction. Large-scale structures appear prominently in the images of the circular 90-deg injection flowfield (Figs. 10a and 10d). Two well-defined features are clearly present in the first image (carbon dioxide injection), and the birth of a third is suggested by the "clump" of fluid appearing just upstream of the middle structure. The vortices present in the helium injector flowfield (Fig. 10d) are nearly as well defined and appear comparable in size to those in Fig. 10a. Freestream fluid is entrained into the jet fluid in the region between the large structures as clearly evidenced in both images. In fact, the helium flowfield contains several "finger-like" intrusions of freestream fluid into the injectant. Small-scale structures are visible throughout the braid regions between the large-scale vortices. Also visible in these images is the separation shock upstream of the injector where boundary-layer separation occurs.

Figures 10b and 10e illustrate the instantaneous flowfield created by the circular 15-deg injector fed with CO_2 and helium, respectively. Immediately apparent in both images is the lack of large-scale protrusions of jet fluid into the freestream as were seen for the circular, transverse injector. Small-scale eddies appear to dominate the interfacial structure in the near field, and freestream fluid does not penetrate into the jet region as dramatically as for the transverse injector. However, an interesting feature common to both of these images is the bow shock. Figures 10a and 10d display rather strong waves as suggested by the near normal shock behavior near the injector wall. In contrast, the waves found in the oblique flowfield are substantially weaker; the disturbances behave almost entirely as oblique waves. Smaller total pressure losses are therefore expected in the oblique injection flowfield than in the transverse injection flowfield, and the Mach number behind the oblique wave will be greater than that associated with the near normal wave in Figs. 10a and 10d. This may affect the mixing that occurs in the interfacial region, depending on the expansion characteristics of the oblique jet, since the mixing layer formed between the jet and freestream is strongly affected by the respective Mach numbers of each stream.[8,9]

The instantaneous elliptical injector flowfield, shown in Figs. 10c and 10f, has characteristics similar to Figs. 10a and 10d, in that large turbulent structures are again very prominent. Once again, freestream fluid appears to be entrained into the jet fluid at a faster rate than for the oblique case (in its near field) due to these large eddies. As in the circular 90-deg flowfield, finger-like intrusions of freestream fluid appear in the helium image, and small-scale eddies grow throughout the braiding regions between large structures in the carbon dioxide case. The bow shocks in these images also behave in a similar manner to the strong waves in Figs. 10a and 10d. A final feature of interest in Fig. 10c is the inclination of the barrel shock region with respect to the horizontal. Compared to Fig. 10a, the barrel shock for the elliptical injector is oriented at a steeper angle. This is thought to be indicative of the reduced orifice dimension in the spanwise direction of the elliptical geometry.

Figures 11a and 11b illustrate top views of the circular and elliptical transverse injectors, respectively. Each image covers approximately 1.4 in. in the streamwise direction and 1 in. in the spanwise direction. The oblique injector has been omitted since the field of view offered little information in this case. Figure 11a shows the injector location, the projection of the bow shock at the laser sheet elevation, and the cross section of the jet. The high-intensity region just downstream of the jet orifice is a cross section of the barrel shock region made visible by the frozen carbon dioxide particles present. Large protrusions of jet fluid into the freestream are clearly visible in this image, and a variety of both large- and small-scale structures appear all along the interface. Several features suggesting mushroom-shaped counter-rotating pairs of vortices are noted.

The image shown in Fig. 11b demonstrates the dramatic nature of the elliptical injector flowfield. The jet spreads very quickly in the lateral direction near the exit compared to the previous figure. This trend of rapid lateral spreading within the elliptical injector flowfield is also suggested by the averaged results presented above. Large quantities of freestream fluid are engulfed by the vortices, as evidenced by the white regions just downstream of the injector. Smaller scale mushroom-shaped structures, indicating the presence of counter-rotating vortical pairs, are also present.

Instantaneous end view images of the flowfields created by the transverse and oblique circular injectors are presented in Fig. 12. Approximate spatial dimensions of each image are 2.9 in. in the spanwise direction and 1.9 in. in the transverse direction. Figure 12a shows the streamwise plane at $x/d_{\text{eff}} = 2$, whereas Fig. 12b is taken at $x/d_{\text{eff}} = 5$. Counter-rotating vortices oriented in the streamwise direction (out of the page) are very prominent features of each image. Additionally, Fig. 12a shows finger-like structures that burst outward into the freestream around the periphery of the jet/freestream interface. These structures are thought to be cross sections of the vortices noticed in the side view images of Fig. 10d. No such structures are apparent in Fig. 12b; this is consistent with the side view image of this flowfield in that large-scale eddies are not found. These end views give insight into the role that the streamwise vortices play in the engulfment of freestream fluid. Clearly, as the pair roll toward each other, freestream fluid fills the region in between and is essentially swallowed into the jet where the small-scale turbulence then takes over the mixing process.

Summary and Conclusions

This investigation into the penetration and mixing associated with three injector geometries produced two-dimensional images yielding global injector flowfield characteristics, details of the transverse and lateral spread of the jets, and qualitative information concerning the structural organization and mixing. Condensed ice crystals in the freestream provided the sites for the Mie scattering technique used. This seeding arrangement, due to the small crystal sizes, provided clear identification of the jet/freestream interface in each of the three visualized flow planes. It should be emphasized that since the present seeding technique is not truly "passive" in nature (due to its dependence on the local thermodynamic conditions), no quantitative mixing interpretations can be made from these images.

A stationary three-dimensional bow shock created by the presence of the injectant fluid is clearly observed in all of the images. Also evident in the images obtained from the transverse injector flowfields using carbon dioxide as the injectant are the barrel shock region and Mach disk of the underexpanded jet. Orientations of the large-scale structures in the two transverse cases indicate that the freestream fluid is moving with a lower velocity tangent to the interface than the injectant fluid.

Increases in jet-to-freestream momentum flux ratio result in increased jet penetration into the freestream for all injectors studied. Injector exit geometry does not substantially affect the transverse penetration of the jet in the near field, while the orientation of the injector with respect to the freestream (i.e., transverse vs oblique) has dramatic effects. Averaged images show that the lateral spreading of the elliptical transverse injector is roughly 25% greater in the near field than the lateral spread associated with the circular transverse injector, indicating that the axis-switching phenomenon noted in previous studies of elliptical jets issuing into quiescent or coflowing environments may be preserved in this flowfield. Injector orientation plays an important role in the strength of the bow shock, with the shocks created by the oblique injector being substantially weaker than those created by the transverse injectors. This translates into a smaller expected total pressure loss in the oblique injector flowfield.

Instantaneous images of the three flow planes show a highly complicated, three-dimensional injection flowfield. Side views illustrate the large-scale eddies present along the jet/freestream interface in the flowfields created by the transverse injectors. These eddies result from both the interfacial strain produced as the jet is rapidly turned downstream and the vorticity present within the jet's boundary layer. They are thought to be the principal contributors to near-field mixing between the injectant and freestream fluids. Small-scale vortices develop in the braiding regions between the large eddies. In the oblique injector flowfield, no large-scale vortices develop along the interface in the near-field region. This is consistent with previous work that indicates that the oblique injector mixes slowly in the near field relative to transverse injectors. Top views of the transverse injector flowfields show

large-scale vortices extending appreciably into the freestream and aiding in mixing the freestream and injectant fluids. Finally, end views illustrate the counter-rotating streamwise vortices generated as the jet exits into the freestream. These structures contribute largely to freestream engulfment by the jet and are present in each flowfield studied. Two dominant types of large-scale motions are thus identified within the near injector regions of transverse injection flowfields: streamwise-oriented counter-rotating vortical pairs and vortices developing at the jet/freestream interface orienting themselves tangent to the interface.

Acknowledgments

The authors would like to acknowledge the contributions of J. Donbar, D. Schommer, C. Smith, and D. Glawe. The long, odd hours required for these experiments were above and beyond the call. Also, support of the air facility personnel and machinists of Building 18 was greatly appreciated.

References

[1]Zukoski, E. E., and Spaid, F. W., "Secondary Injection of Gases into a Supersonic Flow," *AIAA Journal*, Vol. 2, No. 10, 1964, pp. 1689–1696.

[2]Schetz, J. A., and Billig, F. S., "Penetration of Gaseous Jets Injected into a Supersonic Stream," *Journal of Spacecraft and Rockets*, Vol. 3, No. 11, 1966, pp. 1658–1665.

[3]Papamoschou, D., and Hubbard, D. G., "Visual Observations of Supersonic Transverse Jets," *Experiments in Fluids*, Vol. 14, 1993, pp. 468–476.

[4]Rothstein, A. D., "A Study of Normal Injection of Hydrogen into a Heated Supersonic Flow Using Planar Laser-Induced Fluorescence," Los Alamos National Lab., LA-12287-T, Los Alamos, NM, 1992.

[5]Hollo, S. D., McDaniel, J. C., and Hartfield, R. J., "Characterization of Supersonic Mixing in a Nonreacting Mach 2 Combustor," AIAA Paper 92-0093, Jan. 1992.

[6]Fric, T. F., and Roshko, A., "Structure in the Near Field of the Transverse Jet," *Seventh International Symposium on Turbulent Shear Flows*, Stanford Univ., Stanford, CA, 1989, pp. 225–237.

[7]Kamotani, Y., and Greber, I., "Experiments on a Turbulent Jet in a Cross Flow," *AIAA Journal*, Vol. 10, No. 11, 1972, pp. 1425–1429.

[8]Messersmith, N. L., and Dutton, J. C., "An Experimental Investigation of Organized Structure and Mixing in Compressible Turbulent Free Shear Layers," Univ. of Illinois at Urbana–Champaign, UILU-ENG-92-4002, Urbana, IL, 1992.

[9]Clemens, N. T., and Mungal, M. G., "Two- and Three-Dimensional Effects in the Supersonic Mixing Layer," *AIAA Journal*, Vol. 30, No. 4, 1992, pp. 973–981.

[10]Hermanson, J. C., and Winter, M., "Mie Scattering Imaging of a Transverse, Sonic Jet in Supersonic Flow," *AIAA Journal*, Vol. 31, No. 1, 1993, pp. 129–132.

[11]Lee, M. P., McMillin, B. K., Palmer, J. L., and Hanson, R. K., "Planar Fluorescence Imaging of a Transverse Jet in a Supersonic Crossflow," *Journal of Propulsion and Power*, Vol. 8, No. 4, 1992, pp. 729–735.

[12]Smith, S. H., Lozano, A., Mungal, M. G., and Hanson, R. K., "Scalar Mixing in the Subsonic Jet in Crossflow," *AGARD Computational and Experimental Assessment of Jets in Cross Flow*, Winchester, England, UK, 1993, pp. 6.1–6.13.

[13]Mays, R. B., Thomas, R. H., and Schetz, J. A., "Low Angle Injection into a Supersonic Flow," AIAA Paper 89-2461, July 1989.

[14]Fuller, E. J., Mays, R. B., Thomas, R. H., and Schetz, J. A., "Mixing Studies of Helium in Air at High Supersonic Speeds," *AIAA Journal*, Vol. 30, No. 9, 1992, pp. 2234–2243.

[15]Schetz, J. A., Thomas, R. H., and Billig, F. S., "Mixing of Transverse Jets and Wall Jets in Supersonic Flow," *IUTAM Symposium on Separated Flows and Jets*, Novosibirsk, USSR, 1990, pp. 807–837.

[16]Ho, C., and Gutmark, E., "Vortex Induction and Mass Entrainment in a Small-Aspect-Ratio Elliptic Jet," *Journal of Fluid Mechanics*, Vol. 179, 1987, pp. 383–405.

[17]Schadow, K. C., Gutmark, E., Koshigoe, S., and Wilson, K. J., "Combustion-Related Shear-Flow Dynamics in Elliptic Supersonic Jets," *AIAA Journal*, Vol. 27, No. 10, 1989, pp. 1347–1353.

[18]Gutmark, E., Schadow, K. C., and Wilson, K. J., "Noncircular Jet Dynamics in Supersonic Combustion," AIAA Paper 87-1878, June 1987.

[19]Gruber, M. R., and Nejad, A. S., "Development of a Large-Scale Supersonic Combustion Research Facility," AIAA Paper 94-0544, Jan. 1994.

[20]Carroll, B. F., Dutton, J. C., and Addy, A. L., "NOZCS2: A Computer Program for the Design of Continuous Slope Supersonic Nozzles," Univ. of Illinois at Urbana–Champaign, UILU ENG 86-4007, Urbana, IL, 1986.

[21]Clemens, N. T., and Mungal, M. G., "A Planar Mie Scattering Technique for Visualizing Supersonic Mixing Flows," *Experiments in Fluids*, Vol. 11, 1991, pp. 175–185.

[22]Wegener, P. P., and Pouring, A. A., "Experiments on Condensation of Water Vapor by Homogeneous Nucleation in Nozzles," *Physics of Fluids*, Vol. 7, No. 3, 1964, pp. 352–361.

[23]Wegener, P. P., and Parlange, J. Y., "Non-Equilibrium Nozzle Flow with Condensation," *AGARD Recent Advances in Aerothermochemistry*, Oslo, Norway, 1967, pp. 607–634.

[24]Samimy, M., and Lele, S. K., "Motion of Particles with Inertia in a Compressible Free Shear Layer," *Physics of Fluids A*, Vol. 3, No. 8, 1991, pp. 1915–1923.

[25]Adamson, T. C., and Nicholls, J. A., "On the Structure of Jets from Highly Underexpanded Nozzles into Still Air," *Journal of the Aero/Space Sciences*, Vol. 26, 1959, pp. 16–24.

[26]Reynolds, W. C., "Thermodynamic Properties in SI: Graphs, Tables, and Computational Equations for 40 Substances," Dept. of Mechanical Engineering, Stanford Univ., Stanford, CA, 1979.

[27]Keffer, J. F., and Baines, W. D., "The Round Turbulent Jet in a Cross-Wind," *Journal of Fluid Mechanics*, Vol. 15, 1963, pp. 481–496.

[28]McDaniel, J. C., and Graves, J., "Laser-Induced Fluorescence Visualization of Transverse Gaseous Injection in a Nonreacting Supersonic Combustor," *Journal of Propulsion and Power*, Vol. 4, No. 6, 1988, pp. 591–597.